J Mater Sci (2007) 42:5991–5998
DOI 10.1007/s10853-006-1127-z

Preparation of luminescent nanosized $NaEu(MoO_4)_2$ incorporated in amorphous matrix originated from zeolite

Shigeru Suzuki · Munenori Ryo · Tetsushi Yamamoto · Takao Sakata · Shozo Yanagida · Yuji Wada

Received: 17 March 2006 / Accepted: 10 October 2006 / Published online: 6 April 2007

Abstract Novel luminescent material has been prepared by the reaction of Eu^{3+} and molybdate species in the matrix of faujasite (FAU) type zeolite X and successive calcination. Eu^{3+} exchanged FAU was reacted with MoO_3 in the solid-state at 723 K, giving a precursor. By calcining it at 1073 K, different crystalline phases were derived depending on MoO_3-loading levels. Scheelite type crystal of $NaEu(MoO_4)_2$ was formed at high MoO_3-loading levels, whereas europium sodalite was formed at low loading levels. For the former sample, X-ray diffraction analysis and transmission electron microscopy revealed that the nanosized $NaEu(MoO_4)_2$ was dispersed homogeneously within amorphous aluminosilicate matrix originated from FAU. The amorphous particles containing $NaEu(MoO_4)_2$ maintained the original morphology, which the starting FAU particles possessed. The emission intensity of nanosized $NaEu(MoO_4)_2$ in the matrix was one order higher than that of europium sodalite. The emission lifetime of nanosized $NaEu(MoO_4)_2$ (0.39 ms) in the matrix was longer than that of bulk $NaEu(MoO_4)_2$ (0.35 ms) fabricated by conventional solid-state processes.

S. Suzuki (✉)
Tokan Material Technology, 2-1-27, oyodo-kita, Kita-ku, Osaka-shi, Osaka 531-8526, Japan
e-mail: shigeru_suzuki@tomatec.co.jp

M. Ryo · T. Yamamoto · Y. Wada
Material and Life Science, Graduate School of Engineering, Osaka University, 2-1 Yamadaoka, Suita, Osaka 565-0841, Japan

T. Sakata
Research Center for Ultra-High Voltage Electron Microscopy, Osaka University, 7-1 Mihogaoka, Ibaraki, Osaka 567-0047, Japan

S. Yanagida
Center for Advanced Science and Innovation, Osaka University, 2-1 Yamadaoka, Suita, Osaka 565-0841, Japan

Introduction

Luminescent materials have been mainly applied for fluorescent lamps, cathode-ray tubes, and X-ray detectors. Recently, the materials have found further applications in the field of light generation for displays and illumination such as PDP, FED and white LED. [1] Luminescent materials for these applications must generally have small particle size, narrow particle size distribution, non-agglomeration and uniformed shape [2]. These properties should lead to a high screen density, low screen loading and high screen resolution. Therefore, the control of particle morphology is a major research target these days to obtain luminescent materials with improved performance [3].

The luminescent materials are generally inorganic solid-state. In conventional solid-state processes, particle size and shape cannot readily be controlled because high reaction temperature and repeated milling processes result in irregular morphology of the luminescent materials. For this reason, there have been a number of attempts to synthesize fine-grained variations of these materials and thin films by a variety of different techniques such as, chemical vapor deposition [4], combustion synthesis [5], and colloidal reactions [6].

The nanosized luminescent particles in particular have been attractive since the optical properties of nanocrystalline materials differ from those of their bulk counterparts and can be influenced by the particle size [7–10]. However, serious drawbacks of free standing nanosized luminescent particles are their surface defects and marked ability to adsorb moisture and carbon dioxide causing deactivation of

excitation by energy transfer through vibrational excitation [11]. The aggregation of nanosized particles should also cause a problem in handling. To prevent quenching of the luminescence and stabilize nanosized particle aggregation, it is desirable to incorporate the nanosized luminescent particles into optically inert and transparent medium as a host.

From these points of view, we have paid special attention to zeolite as a host for designing nanosized luminescent materials [12–14]. Zeolites are attractive hosts of emitters due to the following reasons: (1) They possess the ability to locate cations uniformly; (2) The cages having unique spatial shapes enable guest species to be hosted stably and separately; (3) They are highly transparent in the UV and visible region; (4) The particle sizes are controllable [15–17] and (5) They possess uniform size and shape. In addition, zeolites are ecological and inexpensive materials.

Rare earth ion-exchanged zeolites have been used as catalysts in the cracking of hydrocarbons for many years. Recently several attentions have been given to zeolites as new luminescent materials [12–14, 18–29]. The studies have been mainly focused on Eu^{3+} and Tb^{3+} exchanged zeolites. Eu^{3+} exchanged zeolite however gave only low quantum yields in its photoluminescence. It was pointed out that the existence of adsorbed and/or coordinated water to exchanged cations and silanol groups in the cages caused deactivation of excitation by energy transfer through vibrational excitation [30]. Therefore, in order to obtain strong emission using zeolites as the host, elimination of coordinating water molecules and silanol groups in their cages is necessary. An effective way reported by Borgmann et al. is to use zeolites as a precursor for Eu^{3+} doped aluminosilicate [22]. This method allowed the synthesis of efficiently emitting europium sodalites from Eu^{3+} and molybdate doped zeolite. This is attributed to the creation of restricted Eu^{3+} environment and the reduction of OH species in the material. Rocha et al. succeeded in observing strong luminescence of Er^{3+}-doped narsarsukite, which was obtained from ETS-10 by a phase transition under calcination at high temperatures above ca. 973 K [24]. Thus, the approach using phase transition of zeolites is an effective way for excluding coordinating water and silanol.

With the aim of designing nanosized luminescent particles within a zeolitic host, we use zeolite matrix for the synthesis of the nanosized luminescent crystal. In addition to excluding coordinating water and silanol group, phase transition of zeolite was taken into consideration for the creation of nanosized luminescent crystal within the host matrix.

In this report, we present a novel synthesis of nanosized $NaEu(MoO_4)_2$ via the reaction of Eu^{3+} and molybdate species in the matrix of faujasite (FAU) type zeolite X and successive calcination. Eu^{3+} was loaded to FAU by ion exchange. The resulting Eu^{3+} exchanged FAU was reacted with MoO_3 in the solid-state and then modified FAU was calcined to derive phase transition. The structure, morphology and emission property were discussed. The effects of MoO_3-loading level on the emission property have been also investigated in terms of the crystal structure derived from phase transition. Furthermore, the results were compared with bulk $NaEu(MoO_4)_2$ fabricated by conventional solid-state process.

Experimental

Preparation

A starting zeolite material was commercially available FAU type zeolite Na-X (NX-110P: Nippon Chemical Industrial, Si/Al = 1.23). The zeolite (30 g) was slurried in 2000 mL of aqueous solution containing 0.04 M $EuCl_3 \cdot 6H_2O$ (Mitsuwa) and stirred at 360 K for 60 min. After the product was separated by filtration, it was washed with deionized water, and dried in air at 393 K. The resulting Eu^{3+} exchanged FAU was mixed with two different amounts of MoO_3 (Taiyo Koko). The mixtures were put on a cordierite ceramics plate and then heated slowly to 723 K in air. After it was heated at this temperature for 10 h, the sample was cooled to room temperature. A part of the resulting sample was heated again at 1073 K for 10 h in air.

For comparison, bulk $NaEu(MoO_4)_2$ was prepared by a conventional solid-state reaction. Constituent powders of Eu_2O_3 (Wako), Na_2CO_3 (Wako), and MoO_3 were dry-mixed with a henschel-type mixer. The mixture was put on a cordierite plate and then heated at 1073 K for 1 h in air.

Measurements

Chemical compositions Eu, Mo, Al, and Si of the prepared samples were determined by inductively coupled plasma analysis (SEIKO Instruments, SPS1700HVR). The content of Na was determined by atomic absorption analysis (Thermo Elemental, SolaarM5). The samples were investigated by powder X-ray diffraction (XRD) for identifying their structures. The XRD profiles were recorded on a Rigaku Model Dmax 2000 diffractometer using CuKα radiation. Thermogravimetric (TG) profiles were measured with a MAC Science MTC1000S. A total weight loss between 298 K and 673 K was employed for calculating the amount of desorbed water.

A scanning electron microscope (SEM) was applied to observe the surface morphology of each sample (HITACHI, S-3000N). A transmission electron microscope

(TEM) and a scanning transmission electron microscope (STEM) were used to determine the microscopic structures. (HITACHI, H-9000). Energy depressive X-ray (EDX) spectroscopy attached to STEM was also applied for elemental mapping (HITACHI, H-800). For TEM and STEM-EDX study, the sample was crushed with glass beads in ethanol solvent with a paint conditioner (Red Devil Inc., 5410). The obtained slurry of the sample in ethanol was dropped onto a copper grid covered by a thin layer of carbon. Particle size distribution was determined by laser diffraction analysis using unified scatter technique (NIKKISO, MICROTRAC HRA). Emission and excitation spectra were obtained with a HITACHI F-4500 at room temperature. In order to compare the emission intensities, the measurements were carried out in a reflectance mode under identical conditions: optical setup, focalization point and illuminated cross-section, sample holder, emission and excitation slits width and the equal volumes of the samples having the same particle size were used in each measurement. Decay profiles monitored at 614 nm were recorded with the photomultiplier coupled to an oscilloscope upon excitation with the third harmonic of a Nd:YAG laser (355 nm).

Results and discussion

Characterization

Chemical analysis of Eu^{3+}-exchanged zeolite gave the following chemical composition of its unit cell: $Na_6Eu_{23}(AlO_2)_{83} \cdot (SiO_2)_{106}$-$nH_2O$. The degree of Eu^{3+} ion-exchange was 83% (denoted as Eu^{3+}-FAU hereafter). The nomenclature of the samples prepared in this study and their chemical analysis are listed together with the calcination temperatures in Table 1. The numbers of molybdenum atoms contained in a unit cell were 17 at lower MoO_3-loading levels (sample l-723) and 42 at higher MoO_3-loading levels (sample h-723), respectively. The molybdenum contents were slightly decreased after calcination at 1073 K (sample l-1073, h-1073) in both systems. This suggests that a small amount of MoO_3 was lost by vaporization.

Their XRD profiles are depicted in Fig. 1. No diffraction patterns of the MoO_3 were detected in the sample l-723 and h-723, suggesting that molybdenum oxide species was present in the sample as a monomer or an oxide cluster. The observed patterns showed only the peaks characteristic of FAU. SEM images of these samples also allowed us to observe only the zeolitic particle of FAU. Therefore, these results revealed that molybdenum oxide species entered into the pore structure of the FAU, probably as monomer or clusters of MoO_3 or ions such as MoO_4^{2-} by calcination at 723 K. The peak intensities were weakened as the amounts of loaded MoO_3 increased, indicating the decrease in the crystallinity of zeolites. This decrease should be attributed to slightly acidic character of MoO_3, which should destroy the FAU structure. These results were consistent with the previous publication [31].

The FAU structure collapsed except for Eu^{3+}-FAU-1073 when the samples were calcined at 1073 K, and formation of new crystalline phases were observed. For the sample l-1073 with low MoO_3-loading, the diffraction pattern showed good agreement with that of europium sodalite (Eu-SOD) having the composition $Eu_4Si_4Al_8O_{24}(MoO_4)_2$ reported by Borgmann et al. [22].

For the sample h-1073 with high MoO_3-loading level, the main diffraction peaks were similar to those of sodium gadolinium molybdenum oxide: $NaGd(MoO_4)_2 \cdot$ (JCPDS no. 25-0828) though the slight formation of Eu-SOD as a by-product was recognized. This revealed that $NaEu(MoO_4)_2$ of scheelite type structure is predominantly formed by loading high amounts of MoO_3. Eu^{3+} and Na^+ share the sites usually occupied by Ca^{2+} in the natural scheelite $CaWO_4$ [32]. Since chemical analysis of the sample h-1073 indicated that the number of Na^+ (6) per unit cell was much less than that of Eu^{3+} (23), it is reasonable to consider that Eu^{3+} (and cation vacancies) replaced Na^+ in the derived

Table 1 Nomenclature, calcination condition, chemical analysis, crystal form and water content of samples

Sample	Calcination temprature (K)	Unit cell formula					Crystal form	Water content (wt%)
		Na	Eu	Mo	Al	Si		
Eu^{3+}-FAU-723	723	6	23	0	82	106	FAU	19.8
l-723	723	6	23	17	81	106	FAU	16.3
h-723	723	6	23	42	81	106	FAU	12.1
Eu^{3+}-FAU-1073	723/1073	6	23	0	83	106	FAU	19.5
l-1073	723/1073	6	23	16	82	106	$Eu_4Si_4Al_8O_{24}(MoO_4)_2^a$	1.8
h-1073	723/1073	6	23	40	80	106	$NaEu(MoO_4)_2$	0.4

$Eu_4Si_4Al_8O_{24}(MoO_4)_2^a$: Europium sodalite reported by Borgmann et al. [22]

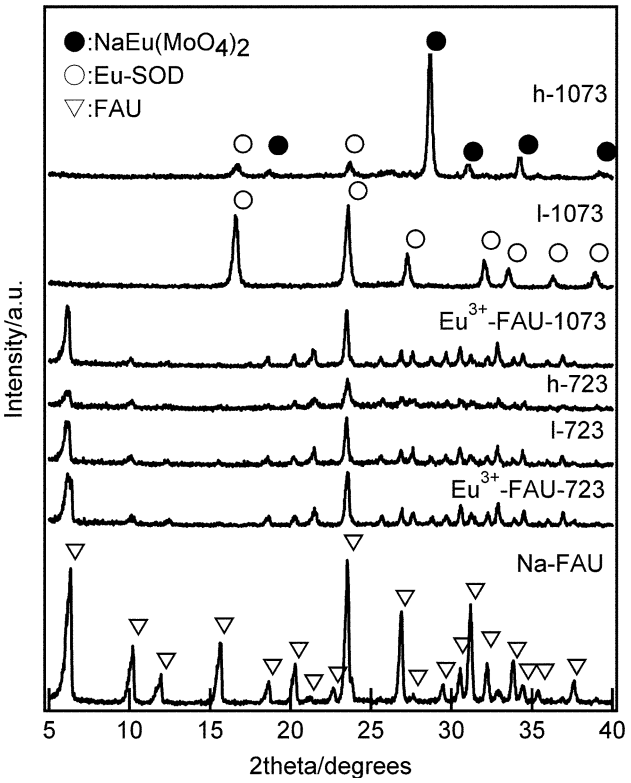

Fig. 1 XRD patterns of the starting Na-FAU and the samples. The sample names are listed in Table 1

scheelite crystal. When molybdates of monovalent and trivalent metal cations crystallize into a scheelite structure with general formula $A^{+1}_{0.5-3x}A^{3+}_{0.5+x}\varphi_{2x}MoO_4$, one trivalent cation is readily replaced by three monovalent cations resulting in the formation of two cation vacancies (φ). Another components originated from FAU, namely Al, and Si should exist as amorphous oxide phase, except for small amounts of Eu-SOD.

The contents of water re-adsorbed in air after calcination confirmed by TG measurements are also listed in Table 1. Eu^{3+}-FAU alone possessed about 20 wt% of re-adsorbed water even after calcination at 1073 K. In the samples l-723 and h-723, the water contents were 16.3 wt% and 12.1 wt%, respectively. Although the insertion of the molybdenum oxide species into Eu^{3+}-FAU was confirmed by XRD measurements, no drastic loss of water was observed. Elimination of water was observed in the samples which underwent phase transition into Eu-SOD (sample l-1073, 1.8 wt%) and $NaEu(MoO_4)_2$ (sample h-1073, 0.4 wt%).

Morphology of the samples

Figure 2 shows the SEM images of the (a) starting Na-FAU; (b) Eu^{3+}-FAU alone (Eu^{3+}-FAU-1073); (c) the sample with low MoO_3 loading levels (l-1073), containing Eu-SOD; and (d) the sample with high MoO_3 loading levels (h-1073), containing $NaEu(MoO_4)_2$. Even after calcination at 1073 K, all the samples maintained zeolitic uniformity and they formed no aggregation. Although thus macroscopic changes were not observed, surface morphology was changed depending on the MoO_3-loading level. Eu^{3+}-FAU alone maintained the original surface

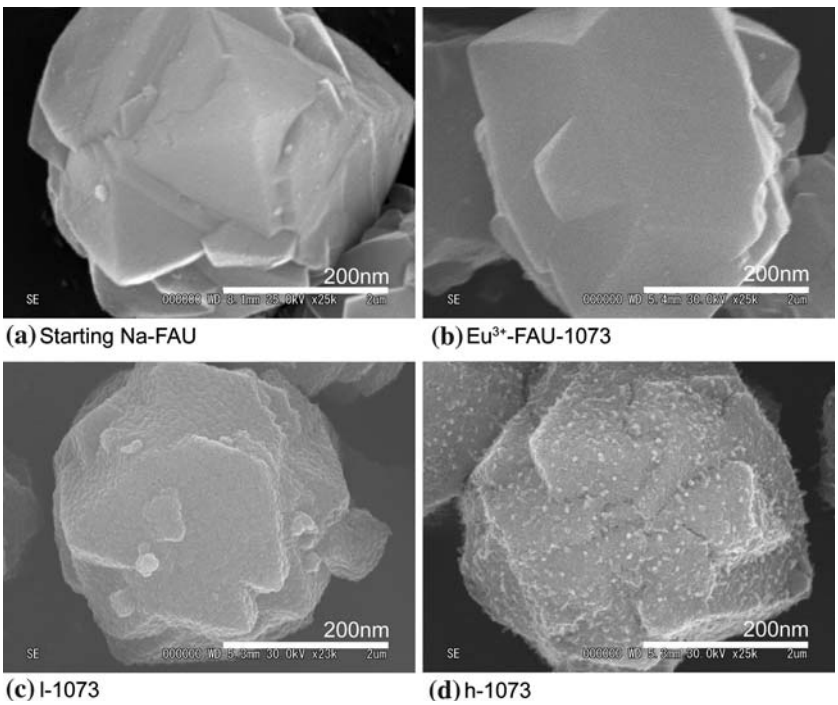

Fig. 2 SEM images of (**a**) Starting Na-FAU; (**b**) Eu^{3+}-FAU-1073; (**c**) l-1073; and (**d**) h-1073

morphology, which the starting FAU particle possessed (Fig. 2b). When MoO_3 was loaded with low levels (sample l-1073), the particle surface was slightly roughened (Fig. 2c). Drastic change was observed when MoO_3 was loaded with high levels (sample h-1073). Fig. 2d indicated that nanosized particles were deposited on the particle surface homogenously. The diameters of these particles were about 30–80 nm.

To investigate these nanosized particles in more detail, TEM observation and elemental mapping using EDX were performed on the specimen of the sample h-1073. Many nanosized particles (dark contrast) surrounded by a bright contrast phase were observed as shown in Fig. 3a. The diameters of these nanosized particles were about 10–80 nm, agreed with the result of the SEM observation. Their STEM image and elemental maps are also depicted in Fig. 3b. The STEM elemental mappings confirmed the presence of Mo and Eu in the nanosized particles and that of Al and Si in the bright contrast phase. In conjunction with the XRD measurements, these nanosized particles and bright contrast phase were identified as $NaEu(MoO_4)_2$ and amorphous aluminosilicate matrix, respectively. Therefore, the sample h-1073 can be regarded as a composite material consisting of nanosized $NaEu(MoO_4)_2$ and amorphous matrix.

The particle size distributions of the sample h-1073 and the starting Na-FAU are depicted in Fig. 4. The particle size distribution was almost unchanged after the sample preparation, indicating that the mono-dispersibility of the starting Na-FAU particles was retained in the resulting composite.

Therefore, the results have led us to a conclusion that an approach using phase transition of zeolites enables us to synthesize nanosized $NaEu(MoO_4)_2$ crystals in the amorphous matrix without forming aggregates. An explanation to this method could be related to the microstructure of zeolite as discussed below. When Eu^{3+} and MoO_3 are loaded into the zeolite preliminarily, crystallization of $NaEu(MoO_4)_2$ proceeds in zeolite cavities, which can offer a limited nano-spaces for crystal formation. Zeolite frameworks act as a wall for inhibiting excess crystal growth, though zeolite is also destroyed by calcination. In contrast, particle morphology cannot be readily controlled by conventional solid-state process. Consequently, using phase transition from zeolite can be considered as an appropriate way for constructing nanosized crystals within amorphous matrix.

Emission properties

Emission spectra of the prepared samples are depicted in Fig. 5. Under irradiation at 396 nm corresponding to the $^7F_0$– $^5L_6$ transition of Eu^{3+}, each sample gave luminescence attributed to the $^5D_0$– $^7F_1$, $^5D_0$– $^7F_2$, $^5D_0$– $^7F_3$, and $^5D_0$– $^7F_4$ transition of Eu^{3+}. A week emission attributed to $^5D_0$– $^7F_0$ transition was observed for h-1073. Fig. 5a

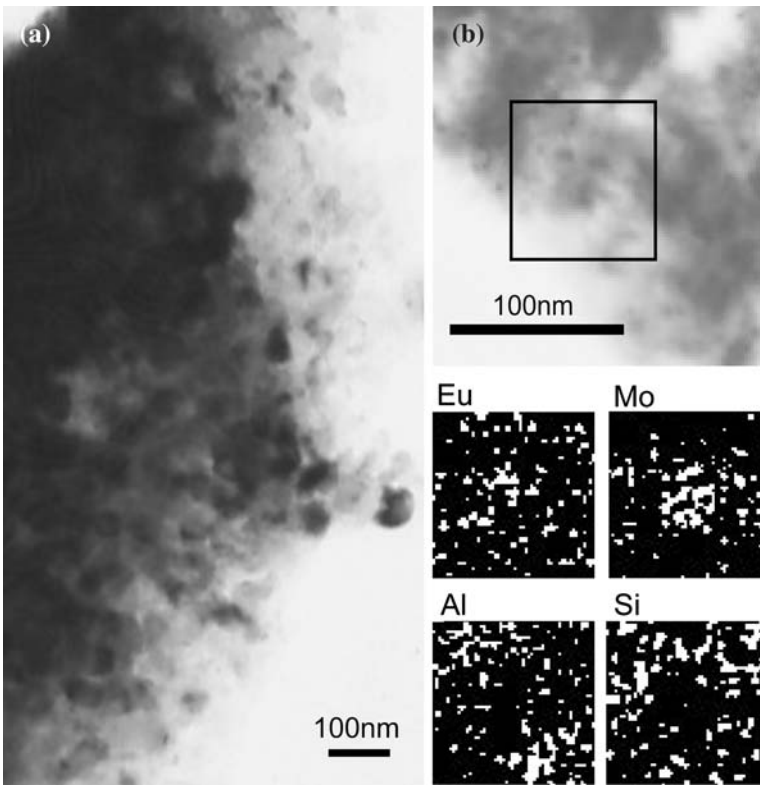

Fig. 3 (**a**) TEM image of specimen of h-1073; (**b**) STEM image and elemental maps of h-1073. Elemental maps of Eu, Mo, Al, and Si were made of the area outlined in the black square

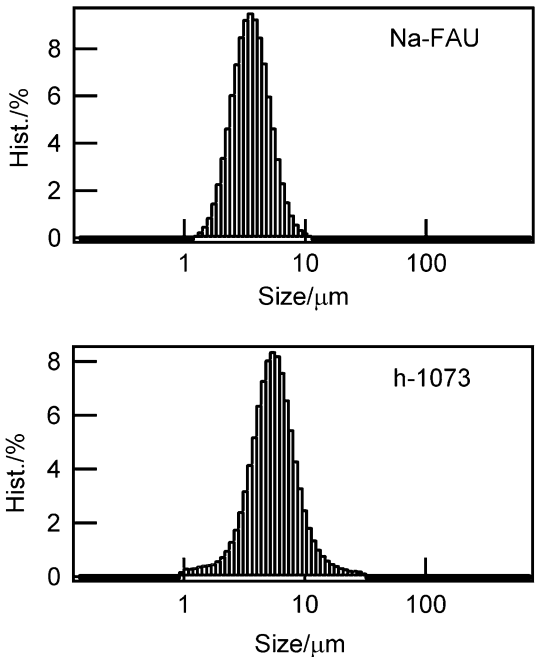

Fig. 4 The particle size distribution of starting Na-FAU and h-1073

clearly shows that the strongest emission intensity was obtained for the sample h-1073 containing nanosized $NaEu(MoO_4)_2$. The weakest emission intensity was observed for the Eu^{3+}-exchanged FAU (Eu^{3+}-FAU-1073), presumably due to re-absorbed water (see Table 1). Eu^{3+} and H_2O molecules should be distributed in the supercage of the FAU. The numbers of Eu^{3+} and H_2O per supercage calculated from chemical and TG analysis were 2.9 and 26, respectively. Thus, Eu^{3+} should be surrounded by 9.0 H_2O molecules, which are well known as a quencher of excited Eu^{3+} if they are located in the first coordination shell of Eu^{3+} [30]. Although elimination of water molecules and silanol groups was attained by phase transition (see Table 1), emission intensity of the sample l-1073 containing Eu-SOD was at least by one order weaker than that of the sample h-1073. Since the numbers of Eu^{3+} per unit cell and particle sizes were similar in the two samples, it can be concluded that luminescent efficiency of the sample h-1073 was higher than that of the sample l-1073. Note that Eu^{3+}-exchanged FAU containing molybdenum as oxides in the pores (sample h-723, Fig. 5b) showed weaker emission in spite of similar chemical composition with that of the sample h-1073. Therefore the observation has led us to a conclusion that formation of nanosized $NaEu(MoO_4)_2$ enhances the emission. The excitation spectrum of the sample h-1073 (Fig. 6) for monitoring the $^5D_0$– $^7F_2$ transition of Eu^{3+} showed a broad ligand(O) to metal(Mo) charge-transfer (LMCT) band and the sharp lines corresponding to $^7F_0$– $^5D_0$, $^7F_0$– ^5L_j, and $^7F_0$– ^5G_j transitions. Intensities of $^7F_0$– $^5L_6$ (Eu^{3+}) transition at

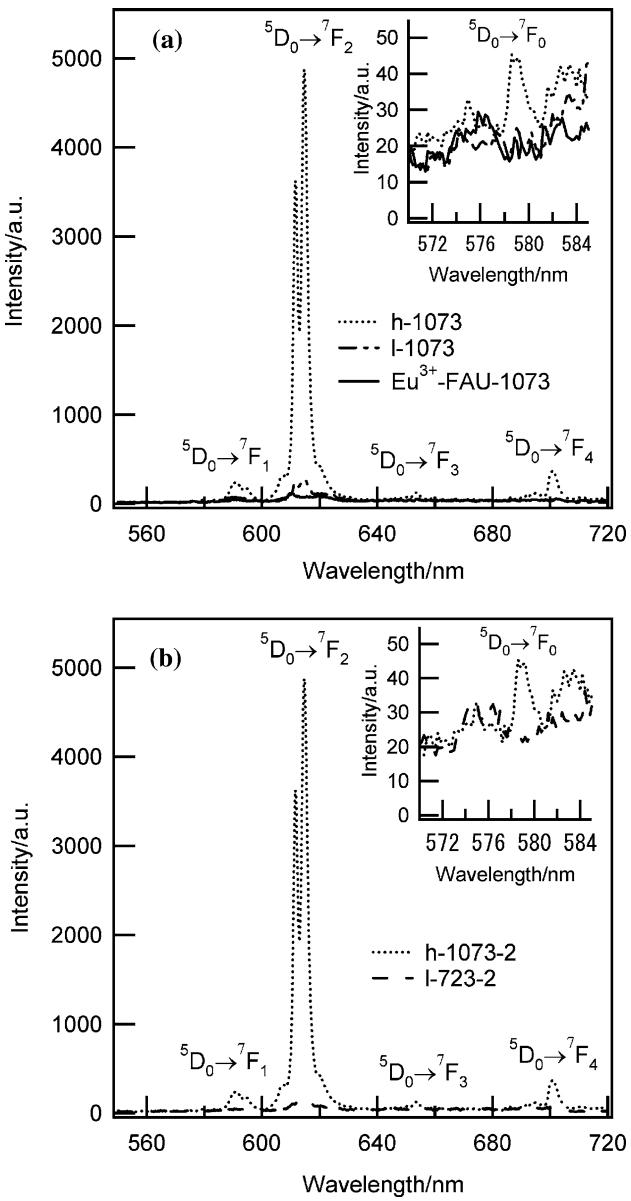

Fig. 5 Emission spectra of the samples. The excitation wavelength was 396 nm

396 nm and $^7F_0$– $^5D_2$ transition (Eu^{3+}) at 463 nm were comparable to the LMCT band.

To compare the emission lifetimes between nanosized $NaEu(MoO_4)_2$ synthesized in the matrix of FAU (sample h-1073) and bulksized $NaEu(MoO_4)_2$ fabricated by a conventional solid-state process, the emission decay curves were monitored at 614 nm ($^5D_0$– $^7F_2$ transition). Figure 7 shows the emission decay curves of both samples. Both of the emission decays followed simple first-order kinetics. The emission lifetimes were 0.39 ms and 0.35 ms for nanosized- and bulksized-$NaEu(MoO_4)_2$, respectively. The fitting errors were within ±0.005. The lifetime value of bulksized-$NaEu(MoO_4)_2$ was consistent with the previous

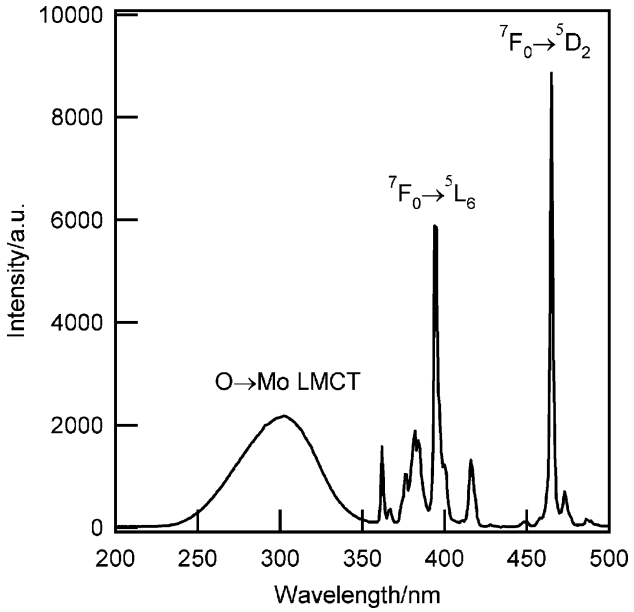

Fig. 6 Excitation spectrum of h-1073. The emission wavelength was 615 nm

publication [33]. Thus, the emission lifetimes of Eu^{3+} in bulk- and nanosized $NaEu(MoO_4)_2$ were very similar. The emission lifetimes are in general decreased when the particle size is decreased [34, 35]. This can be attributed to non-radiative relaxation caused by surface defects and hydrated or carbonated species that act as quenching centers. Because the lifetime τ is described as $(\tau_{rad} + \tau_{nrad})^{-1}$, where τ_{rad} and τ_{nrad} are the radiative rate and the non-radiative rate, respectively, when the surface area increases with decrease of particle size, more defects and hydrated or carbonated species would be formed on the surface, with an

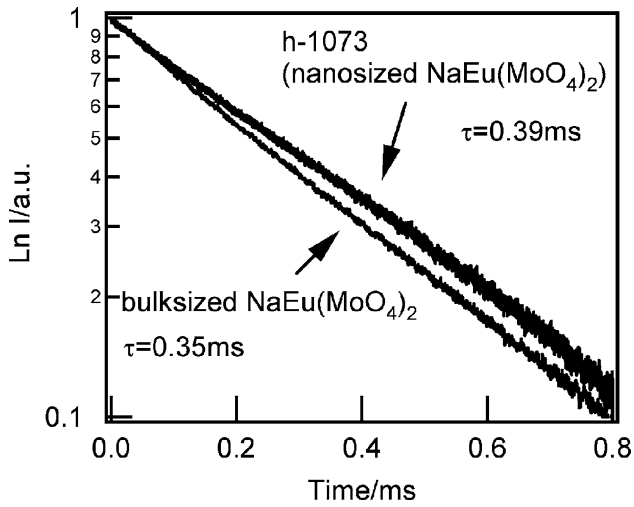

Fig. 7 Emission decay curves monitored at 614 nm of h-1073 and bulk-sized $NaEu(MoO_4)_2$ upon excitation with the third harmonic of a Nd:YAG laser (355 nm)

increased non-radiative rate, the lifetime turns shorter accordingly. Therefore, this observation indicates that the amorphous matrix originated from FAU coating the surfaces of the nanosized $NaEu(MoO_4)_2$ crystals suppress the non-radiative relaxation.

In contrast, conventional fabrication route is via a grinding or milling process in order to obtain fine particle size. This introduces defects into surface and hydrated or carbonated species into surface. Typically, as particles are ground below about 3 μm there is a substantial drop-off in luminescence efficiency [36]. Therefore, this novel route for preparation of nanosized luminescent material within the amorphous matrix via phase transition of zeolites proves to be advantageous in controlling the particle morphology and improving the emission property.

Conclusions

We have prepared first nanosized $NaEu(MoO_4)_2$ in the matrix of faujasite (FAU) type zeolite X by incorporating MoO3 in Eu^{3+} exchanged FAU and subsequent calcination. The sample particles maintained zeolitic uniformity after phase transition and they formed no aggregation. The nanosized $NaEu(MoO_4)_2$ was dispersed homogeneously within amorphous aluminosilicate matrix originated from FAU. Strong emission intensity was obtained from the nanosized $NaEu(MoO_4)_2$. The emission decay profiles have revealed that nanosized $NaEu(MoO_4)_2$ in the matrix provides with high emission efficiency, being comparable to bulk $NaEu(MoO_4)_2$ fabricated by conventional solid-state processes. This suggests that amorphous matrix suppresses non-radiative relaxation by coating the surface of nanosized $NaEu(MoO_4)_2$ crystals. Consequently using phase transition from zeolite can be considered as an appropriate way for constructing nanosized strong luminescent material within amorphous matrix. It is expected that further optimizations of the syntheses by changing Na/Eu ratio of Eu^{3+} exchanged FAU, and co-exchanging with other cation would enhance the emission efficiency.

Acknowledgement The authors would like to thank the members of Analytical Laboratory of Tokan Material Technology Co., Ltd. for help with the chemical analysis. This work was supported by a Grant-in-Aid for Scientific Research (No. 12450345) and a Grant-in-Aid for Scientific Research Areas (417) (No. 15033245) from the Ministry of Education, Culture, Sports, Science and Technology (MEXT) of the Japanese Government.

References

1. Jüstel T, Nikol H, Ronda C (1998) Angew Chem Int Ed 37:3085
2. Vecht A, Gibbons C, Davies D, Jing XP, Marsh P, Ireland T, Silver J, Newport A, Barber D (1999) J Vac Sci Technol B 17:750

3. Feldmann C, Jüstel T, Ronda C, Schmidt PJ (2003) Adv Funct Mater 13:511
4. McKittrick J, Bacalski CF, Hirata GA, Hubbard KM, Pattillo SG, Salazar KV, Trkula M (2000) J Am Ceram Soc 83:1241
5. Ye T, Zhao GW, Zhang WP, Xia SD (1997) Mater Res Bull 32:501
6. Lee MH, Oh SG, Yi SC (2000) J Colloid Interface Sci 226:65
7. Bhargava RN, Gallagher D, Welker T (1994) J Lumin 61:275
8. Bhargava RN (1996) J Lumin. 70:85
9. Weller H (1993) Angew Chem 105:43
10. Alivisatos AP (1996) Science 271:933
11. Capobianco JA, Vetrone F, D'Alesio T, Tessari G, Speghini A, Bettinelli M (2000) Phys Chem Chem Phys 2:3203
12. Wada Y, Okubo T, Ryo M, Nakazawa T, Hasegawa Y, Yanagida S (2000) J Am Chem Soc 122:8583
13. Ryo M, Wada Y, Okubo T, Nakazawa T, Hasegawa Y, Yanagida S (2002) J Mater Chem 12:1748
14. Ryo M, Wada Y, Okubo T, Hasegawa Y, Yanagida S (2003) J Phys Chem B 107:11302
15. Charnell JF (1971) J Crystal Growth 8:291
16. Schoeman BJ, Sterte J, Otterstedt JE (1994) Zeolites 14:110
17. Persson AE, Schoeman BJ, Sterte J, Otterstedt JE (1994) Zeolites 14:557
18. Baker MD, Olken MM, Ozin GA (1988) J Am Chem Soc 110:5709
19. Kynast U, Weiler V (1994) Adv Mater 6:937
20. Rosa ILV, Serra OA, Nassar EJ (1997) J Lumin 72:532
21. Alvaro M, Fornes V, Garcia S, Scaiano JC (1998) J Phys Chem B 102:8744
22. Borgmann C, Sauer J, Jüstel T, Kynast U, Schüth F (1999) Adv Mater 11:45
23. Chen W, Samynaiken R, Huang Y (2000) J Appl Phys 88:16
24. Rocha J, Carlos LD, Rainho JP, Lin Z, Ferreira P, Almedia RM (2000) J Mater Chem 10:1371
25. Jüstel T, Wiechert DU, Lau C, Sendor D, Kynast U (2001) Adv Funct Mater 11:105
26. Sendor D, Kynast U (2002) Adv Mater 14:1570
27. Dexpert-Ghys J, Picard C, Taurines A (2001) J Inclusion Phenom Macrocyclic Chem 39:261
28. Ananias D, Ferreira A, Rocha J, Ferreira P, Rainho JP, Morais C, Carlos D (2001) J Am Chem Soc 123:5735
29. Schmechel R, Kennedy M, von Seggern H, Winkler H, Kolbe M, Fischer RA, Xaomao L, Benker A, Winterer M, Hahn H (2001) J Appl Phys 89:1679
30. Hazenkamp MF, van der Veen AMH, Feiken N, Blasse G (1992) J Chem Soc Faraday Trans 88:141
31. Thoret J, Man PP, Fraissard J (1995) J Chem Soc Faraday Trans 91:1037
32. Schieber M, Holmes L (1964) J Appl Phys 35:1004
33. Macalik L, Hanuza J, Macalik B, Strek W (1996) Eur J Solid State Inorg Chem 33:397
34. Wei-Wei Z, Mei X, Wei-Ping Z, Min Y, Ze-Ming Q, Shang-Da X, Garapon C (2003) Chem Phys Lett 376:318
35. Capobianco JA, D'Aleso T, Tessari G, Speghini A, Bettinelli M (2000) Phys Chem Chem Phys 2:3203
36. Hase T, Kano T, Nakazawa E, Yamamoto H (1990) Adv Electron Electron Phys 79:271